ACS APPLIED MATERIALS & INTERFACES

Letter

www.acsami.org

Very High Laser-Damage Threshold of Polymer-derived Si(B)CN-Carbon Nanotube Composite Coatings

R. Bhandavat,[†] A. Feldman,[‡,§] C. Cromer,[‡] J. Lehman,[‡] and G. Singh[†,*]

[†]Department of Mechanical and Nuclear Engineering, Kansas State University, Manhattan, Kansas 66506, United States

[‡]National Institute of Standards and Technology, 325 Broadway, Boulder, Colorado 80305, United States

[§]Colorado School of Mines, 1500 Illinois Street, Golden, Colorado 80401, United States

Supporting Information

ABSTRACT: We study the laser irradiance behavior and resulting structural evolution of polymer-derived silicon−boron−carbonitride (Si(B)CN) functionalized multiwall carbon nanotube (MWCNT) composite spray coatings on copper substrate. We report a damage threshold value of 15 kWcm^{-2} and an optical absorbance of 0.97 after irradiation. This is an order of magnitude improvement over MWCNT (1.4 kWcm^{-2}, 0.76), SWCNT (0.8 kWcm^{-2}, 0.65) and carbon paint (0.1 kWcm^{-2}, 0.87) coatings previously tested at 10.6 μm (2.5 kW CO_2 laser) exposure. Electron microscopy, Raman spectroscopy, and X-ray photoelectron spectroscopy suggests partial oxidation of Si(B)CN forming a stable protective SiO_2 phase upon irradiation.

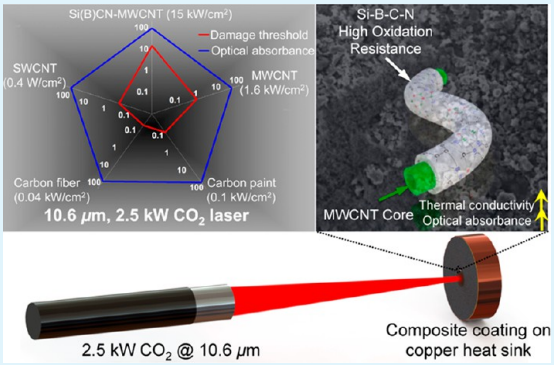

KEYWORDS: *carbon nanotubes, optical coatings, polymer-derived Si(B)CN, laser radiometry*

INTRODUCTION

Copper cone-type thermal calorimeters (or thermal detectors) are commonly used as measurement standards for calibration of high-power infrared lasers used by the military and laser-based manufacturing companies. The inside surface of the copper cone is coated with a radiation-absorbent material to convert the incident radiation energy into thermal energy (conduction). An optimal coating material is desired to possess several functional properties for accuracy and proper working of the detector, which includes: (a) high thermal conductivity for effective transmission of absorbed heat to the substrate,[1,2] (b) zero reflectivity in the visible to infrared spectrum for accurate response and to prevent coating damage due to radiation attenuation,[3] (c) low thermal mass of the coating for higher responsivity,[3,4] and (d) high visual damage threshold (mainly for high power lasers).[1] Additionally, physical properties such as (a) forming a uniform and optimum coating thickness on the desired surface, (b) adhering and forming a stable coating against adverse handling and test conditions,[2] and (c) morphology that allows maximum surface area contact with the substrate are also desired.[5−8]

To this end, a variety of coating materials have been investigated including carbon paint and black metallic coatings (such as the gold black), because of absorption over a broad wavelength range (up to 40 micrometers).[9−14] In spite of having low thermal mass, these coating materials are not suitable for high-power laser radiometry because of their poor laser damage threshold (or low oxidation resistance) and non-uniform spectral response with reflectance reaching as high as 10−20%.[15−20] Recent studies have highlighted the potential of single (SWCNT) and multi-walled carbon nanotubes (MWCNTs) as a durable radiation absorbing material.[1,15−20] MWCNT-based coatings are more promising, because of their broad and uniform spectral absorbance from visible to IR wavelengths, high thermal conductivity, and a laser damage threshold of approximately 15 kW cm^{-2} at 1.06 μm exposure (compared to 7.1 kW cm^{-2} for SWCNTs).[20] However, MWCNTs experience greater damage at 10.6 μm exposure with a reduced damaged threshold value of only 1.4 kWcm^{-2} and 76 % absorption efficiency.[20]

One way to improve the laser damage resistance of MWCNTs (at 10.6 μm exposure) would be to functionalize their surfaces with a high oxidation resistant material such as the polymer-derived Si(B)CN ceramic.[22] Polymer-derived Si(B)CN, which is produced by controlled thermal decomposition (pyrolysis) of liquid polymer (such as boron modified polysilazane) is chemically stable up to temperatures as high as 1500 °C.[23] Polymeric precursor can be readily interfaced with CNTs to yield a core/shell type composite structure upon pyrolysis. Apart from improved oxidation resistance, the core/shell composite is also likely to exhibit high thermal conductivity and optical absorbance contributed by both the nanotube core and graphene like carbon inherently present in Si(B)CN ceramic shell.[24−28] Also, the one pot-synthesis of

Received: November 19, 2012
Accepted: March 11, 2013
Published: March 19, 2013

Si(B)CN-nanotube composite will make it relatively easy to be prepared in large quantities (gram levels), which makes it feasible for laminating any desired substrate of large area using simple spray coating techniques, including the surface of a large laser thermal detector. Therefore, we had good reason to prepare and test spray-coatings of Si(B)CN-MWCNT composite for potential application in high-power radiometry, particularly at 10.6 μm exposure.

EXPERIMENTAL PROCEDURE

Composite Material and Coating Preparation. Coating material was prepared by dispersing 1.0 g of MWCNTs (Bayer Material Science) in 125 mL of toluene by sonication (Branson 2510) for 30 min. This was followed by drop-wise addition of 10.0 g boron-modified polymeric precursor (prepared by use of commercially available polyurea(methylvinyl) silazane (Ceraset, KiON Specialty Polymers, Charlotte, NC) and tri-methyl borate (Alfa Aesar)) with stirring for 24 h followed by slow drying it at 80 °C in an inert atmosphere. On pyrolysis at 1100 °C, this resulted in a core-shell structured, Si(B)CN-MWCNT composite. Detailed step-by-step synthesis is described in our recent work.[22,29] The composite material was gently crushed using mortar-pestle to obtain a fine powder (approximately 1 to 2 μm in size, as determined by the SEM). It was then dispersed in toluene (ACS reagent) and sonicated for 1 h to obtain a dispersion. As shown in Figure 1, the dispersion was carefully

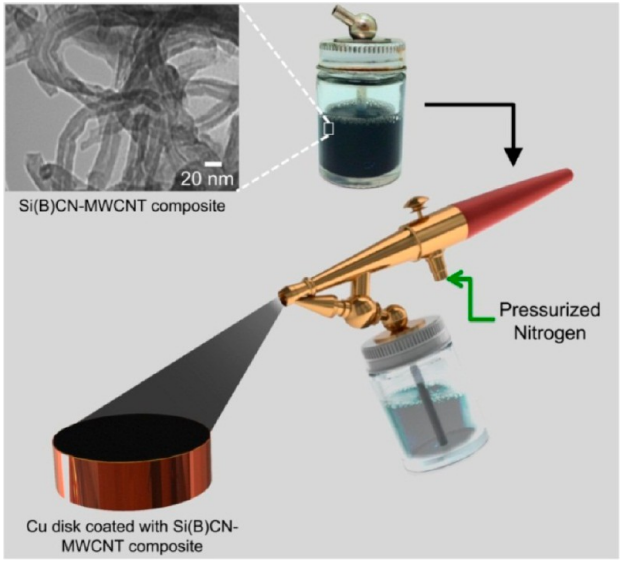

Figure 1. Schematic representation of the spray coating process (Inset is the TEM image showing shell/core structure of the Si(B)CN-MWCNT composite). Uniformly dispersed Si(B)CN-MWCNT nanowires in toluene solution were spray coated using an air brush technique. The coated specimen were then baked overnight at 100 °C for curing.

sprayed on copper substrates by use of an airbrush (model Paasche-H#1) at 15 psi of nitrogen gas. The spraying was done with longitudinal passes (with a single pass lasting for approximately 5 s followed by 10 s of break) while the substrate surface temperature was raised to 80 °C. Frequent stops between the passes allowed the solvent to evaporate and thereby form a uniform compact coating. Spray coating was carried out until the appropriate dark black coating thickness was visually realized with an approximate thickness of 10 μm. The coated copper test specimens were then maintained at 100 °C on a hot plate for 12 h to ensure removal of volatile entities.

The coatings were prepared on two different substrate types: (a) a copper circular disk (weighing 600 grams) with 76 mm diameter and 13.6 mm thickness and, (b) a rectangular copper plate with dimensions 24 mm × 62 mm and 0.75 mm thickness.

EXPERIMENTAL SETUP

The coated copper test specimens were used for studying thermal damage threshold at constant wavelength of 10.6 μm produced by CO_2 laser at increasing power densities of 4, 8, 12, and 15 kW cm^{-2}. Details on the laser experimental set-up are available in reference.[19] Disk specimens received 10 s exposure, whereas copper plate specimens were exposed for 2 s. Typically, a laser thermal detector test setup has a flowing-water jacket to absorb the heat transferred from laser to copper substrate via the coating material. This flowing water also acts as an infinite sink for the heat transferred. This set-up is rather complex and is not feasible for small-scale damage-threshold-testing; hence we utilized a copper disk with large mass (as a heat sink) as a closest representation of the actual calorimeter cone. The coatings prepared on copper plate specimen are likely to experience more damage due to lesser heat dissipation by the substrate because of its low thermal mass (plate specimens weighed approximately ~11 g).

The exposed and unexposed areas of the coatings were analyzed and compared by use of scanning electron microscopy (SEM), Raman and X-ray photoelectron spectroscopy (XPS). SEM analysis of the irradiate areas was done by use of Carl Zeiss EVO low vacuum SEM operating at 5 kV with 25 mm (low resolution) and 10 mm (high resolution) working distance. Specular reflectance of the material was measured from the exposed and unexposed areas (disk specimen) by use of a NIST customized test setup. Briefly, a 10.6 μm CO_2 laser with a 3 mm diameter beam measured at 1.137 W incident power was reflected at approximately 45° from the specimen surface. The power of the reflected beam was detected by use of a thermopile photodetector. To ensure the beam alignment, the beam was first reflected off of a molybdenum mirror, and then replaced with the Si(B)CN-MWCNT coated disk specimen. This specimen was mounted on a translation stage in order to maintain the aligned angle as measurements at different spots were performed. Broadband reflectance measurements for the mid-IR range were carried out by use of Thermo Fisher Nicolet 6700 FT-IR Spectrometer in the ATR mode. Raman spectra were collected on HORIBA LabRAM ARMIS spectrometer using 17 mW HeNe laser source (632.8 nm wavelength (1.96 eV)). The spectra were collected using a 100 X NIR objective lens (theoretical spot size: 842 nm), 200 μm confocal hole, 150 μm wide entrance slit, 600 gr/mmgrating. The surface chemistry of the coating was studied by use of PHI Quantera SXM (ULVAC-PHI, Inc) and monochromatic Al Kα X-radiation with beam size <9 μm. Following a survey scan, a 15-minute high-resolution scan was performed in the major elemental peaks' energy window.

RESULTS AND DISCUSSION

Electron Microscopy. The effect of incremental laser power on coating morphology can be observed in corresponding electron microscopy images. As the copper disk specimen has comparatively better heat dissipation (acting as a large heat sink due to its large thermal mass) than the plate specimen, the coating on disk specimen is expected to withstand much higher power densities and longer periods without damage. Hence, the characterization data is presented in a manner to show incremental coating damage i.e., data from the disk specimen are presented first (Figures 2 and 3) followed by copper plate specimen (Figures 4 and 5).

At low magnifications, the non-irradiated coating surface exhibited a structurally stable and porous morphology with interconnected particles. MWCNTs are believed to provide the reinforcement to the composite coating by holding porous

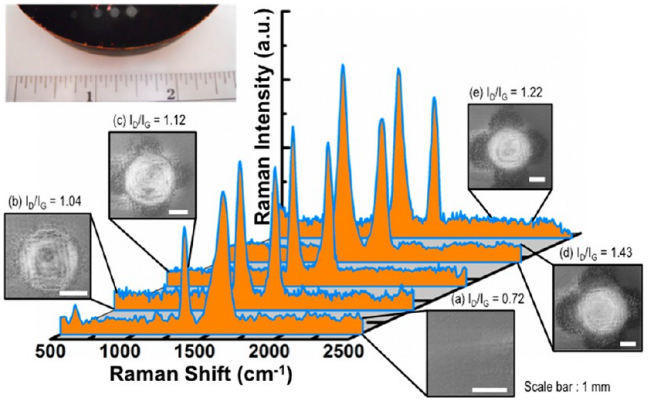

Figure 2. Normalized Raman spectra of Si(B)CN MWCNT coatings exposed to laser irradiance at (a) 0 (unexposed), (b) 4, (c) 8, (d) 12, and (e) 15 kW cm^{-2} for 10 seconds respectively, along with the corresponding SEM micrographs. Scale bar is 1 mm. Insert (top left) is the digital camera image of the specimen.

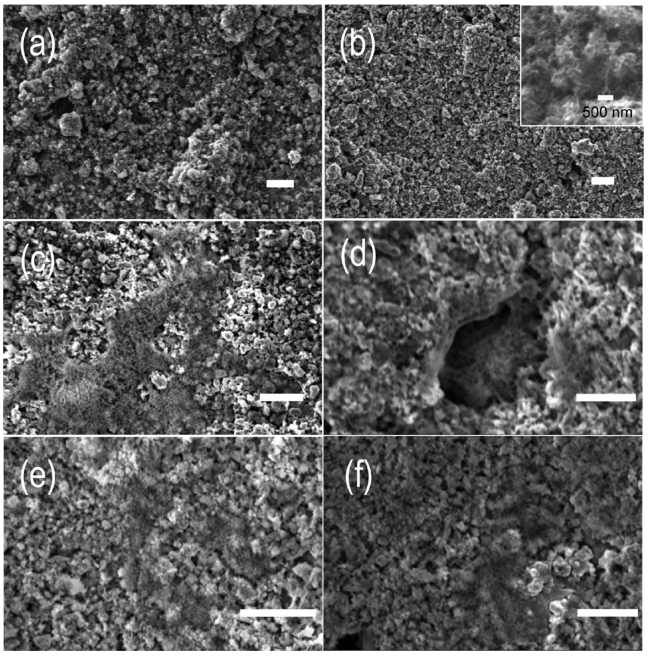

Figure 3. (a, b) SEM images of the "as-prepared" coating on copper disk specimen. (c–f) SEM images from the coating area irradiated at 4, 8, 12, and 15 kW cm^{-2} for 10 s, respectively. Image d seems out of focus because of the coating height difference. Scale bar is 5 μm in all images.

ceramic on to the copper substrate under harsh testing conditions.

The laser-irradiated region of the coating appeared as a bright spot (SEM image charging), whereas the unexposed areas were relatively dark in both the disk (Figure 2) and plate (Figure 4) specimens. For the disk specimen, the transition from non-irradiated to irradiated spot was prominently noticeable (Figure 2a–e). This observation suggests partial oxidation of the ceramic (either Si_3N_4 / SiC in the coating transforming to SiO_2) or burning of partially coated MWCNTs when compared to the "as-prepared" coating, shown in panels a and b in Figure 3. For the 4 kW cm^{-2}, 10 s irradiance (Figure 3c), as much as 70 % of the spot appeared bright. The irradiated spots with 8 and 12 kW cm^{-2} exposure showed

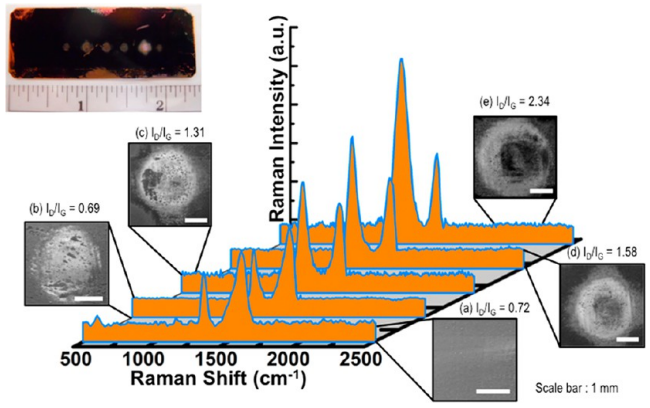

Figure 4. Normalized Raman spectra of Si(B)CN-MWCNT coatings exposed to laser irradiance at (a) 0 (unexposed), (b) 4, (c) 8, (d) 12, and (e) 15 kW cm^{-2} for 2 s, respectively, with the corresponding low-magnification SEM micrographs. Scale bar is 1 mm. Inset (top left) is the digital camera image of the plate specimen.

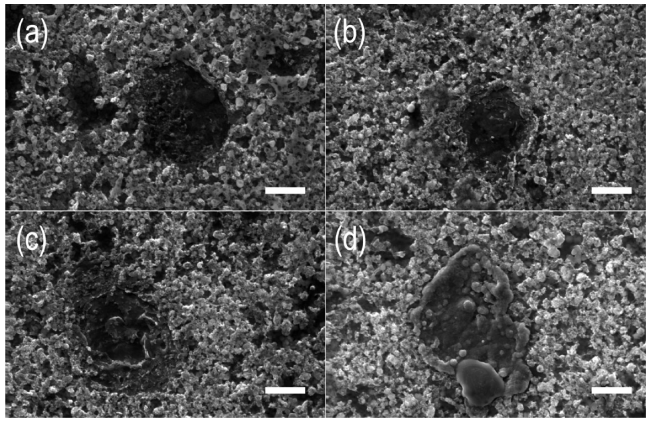

Figure 5. SEM micrographs showing laser-irradiated areas of the coating for copper plate specimen at (a) 4, (b) 8, (c) 12, and (d) 15 kW cm^{-2} for 2 s exposure. Scale bar is 5 μm in all images.

extension of the bright area to about 95 percent. At higher magnifications, Figure 3d , e, these darker areas showed presence of ceramic-coated MWCNT mesh like morphology. The spot at 15 kW cm^{-2} (Figure 3f) appeared similar to that of 12 kW cm^{-2}, and no new changes could be observed in the coating's morphology.

SEM images from the copper plate specimen are compared in Figures 4 and 5. The "as-prepared" coating looked similar to the one on disk specimen (Figure 3a). The irradiated spot at 4 kW cm^{-2} (Figures 4b and 5a) revealed bright areas with some discontinuities. The surface of these discontinuities (gaps) appeared uniform and smooth with intermittent mesh of interconnected ceramic-coated MWCNTs. These gaps are believed to originate from volume changes induced in the composite material because of an abrupt and intense heat generation on coating top surface during continuous laser exposure. As a result, the top layer experienced cracks and increased discontinuities due to increased volume change compared to the inner layer or bottom regions, thereby forming two layers with distinct appearance. We believe that this issue of differential heating could be addressed by optimizing composite coating thickness, which can be a subject of future research.

dx.doi.org/10.1021/am302755x | ACS Appl. Mater. Interfaces 2013, 5, 2354–2359

SEM images also showed round and isolated particles (size less than 1 μm) that are most likely to be the hard ceramic phase. The area irradiated at higher laser density of 8 kW cm^{-2} (Figure 5b) exhibited major transition in the discontinuity regions. Unlike smooth gaps observed for lower laser power densities, this spot showed fused-in/solidified liquid-type of morphology. Further, at 12 kW cm^{-2} exposure (Figure 5c), large isolated gaps (10−20 μm) in the coating with solidified liquidlike texture were observed, whereas at the 15 kW cm^{-2} (Figure 5d) exposure, these gaps appeared more uniform. Remarkably, still under these conditions, the coating was found to be relatively stable and intact on the substrate. The bright appearing spots realized as either SiO_2 or burned nanotubes appeared more pronounced. These observations confirm that composite coatings on test copper plate specimen suffered more severe damage due to low thermal mass of the substrate and insufficient cooling.

Raman Spectroscopy. Raman spectroscopy is a sensitive, nondestructive and non-invasive technique and hence qualifies for studying the evolution of carbon structure (sp^3- and sp^2-type carbon) in the irradiated area. The characteristic "D" and "G" peaks signify the presence of sp^3- and sp^2-type carbon bonds in composite coatings, respectively. Hence, the origin of D-peak collectively corresponds to stretching of Si−C and defect sites in MWCNTs, whereas the G peak corresponds to C═C (graphitic) bonds in the coating material. As shown in Figures 2 and 4, existence of D peak (1330−1356 cm^{-1}) and G peak (1580−1595 cm^{-1}) are invariably observed for all exposures. For the disk specimen, the I_D/I_G ratio increased from 0.72 from the unexposed area to 1.43 from 12 kW cm^{-2} and 1.22 from the 15 kW cm^{-2}, 10 s irradiated spot. And for the plate specimen, the I_D/I_G ratio was 2.34 from the spot that received 15 kW cm^{-2}, 2 s exposure. Hence, almost a linear effect of increasing laser power density on Raman I_D/I_G ratio was observed, suggesting increased defects in sp^2-bonded graphitic carbon with irradiated power. These results also suggest that even under the influence of high irradiance, the graphitic (free) carbon in Si(B)CN is preserved and MWCNTs in the coatings are protected.

Detailed analysis and comparison of the spectrum collected for laser-irradiated spots and as-prepared coatings provided further understanding of structural changes in the carbon structure. As shown in Table 1 for the copper disk specimen, G band (or peaks) experienced a blue shift from ~1584 to ~1593 cm^{-1}, suggesting that the graphitic carbon or the MWCNTs experienced compressive stresses, probably due to change in volume of the surrounding ceramic matrix upon irradiation (also observed in SEM images).[24,26] The calculated ratios of I_D/I_G (summarized in Tables 1 and 2) for the irradiated spots showed a linear increase with increasing laser-power density, suggesting increasing defect sites in sp^2-bonded graphitic carbon in the coatings. The 2D band in the spectra was not analyzed because of their weak intensities.

Table 1. Dependence of I_D (intensity of D-peak) and I_D/I_G (Intensity ratio of D and G peak) as Observed in the Raman Spectra for the Disk Specimen, On the Incident Laser Irradiation Power Density[a]

laser power density (kW cm^{-2})	D peak (cm^{-1})		G peak (cm^{-1})		
	position	FWHM	position	FWHM	I_D/I_G
unexposed	1333	40.2	1584.9	86.4	0.72
4	1351.2	58.5	1585.2	56.9	1.04
8	1351.5	47.3	1587.4	59.3	1.12
12	1334.5	81.5	1593	71.7	1.43
15	1356.2	69.8	1592.1	51.4	1.22

[a]Accuracy in wavenumber measurement was approximately ±1 cm^{-1}. Incident power density was measured to an accuracy of approximately ±10 %.

Table 2. Dependence of I_D and I_D/I_G as Observed in the Raman Spectra for the Plate Specimen, On the Incident Laser Irradiation Power Density[a]

laser power density (kW cm^{-2})	D peak (cm^{-1})		G peak (cm^{-1})		
	position	FWHM	position	FWHM	I_D/I_G
unexposed	1331.7	42.7	1588.8	94.7	0.72
4	1335.2	48.1	1581.7	78.2	0.69
8	1335.2	71.8	1588.8	65.4	1.31
12	1333.5	64.8	1594.1	64	1.58
15	1338.8	97	1580	49.1	2.34

[a]Accuracy in wavenumber measurement was approximately ±1 cm^{-1}. Incident power density was measured to an accuracy of approximately ±10 %.

Reflectance measurements. The measured reflected power with reference to the incident power of 1.137 W laser (15 second pulse) is plotted against time in Figure 6a. The reflectance from the as-prepared Si(B)CN-MWCNT coatings was 1.3 × 10^{-3} ± 2.5 × 10^{-6} W, implying high optical absorption (99.87 %) at 10.6 μm wavelength. As anticipated, increasing magnitude of reflected power is observed from areas that were exposed to higher laser irradiance. Reflected power remained unchanged for 4 and 8 kW cm^{-2} irradiated spots, whereas for the 12 and 15 kW cm^{-2} irradiated spots showed close to 98 % absorption.

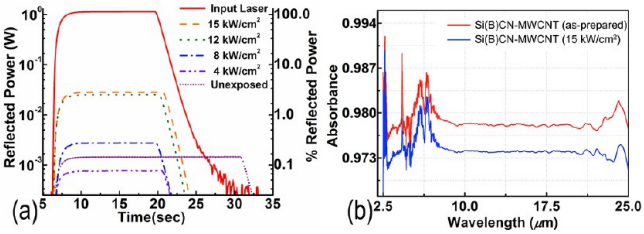

Figure 6. (a) Measured reflected power profiles for the incident laser of 1.137 W at 10.6 μm wavelength from various irradiated areas on the coating for the copper disk specimen. Peak power measurements made with less than 0.5% variance. (b) Mid-IR range spectral absorption response of Si(B)CN-MWCNT coating before and after irradiation at 15 kW cm^{-2} for 10 s.

Further, the adaptability of the composite coatings for longer-wavelength (mid-IR) range was studied by spectral absorption measurements. Comparison of spectral absorption signal from the as-prepared and irradiated areas (Figure 6b) showed high absorption even at longer-wavelengths. Strikingly, even after the damage inflicted by high laser irradiance (15 kW cm^{-2}), the coating maintained a spectral absorption at about 0.97. Change in the chemical structure of ceramic (oxidation) may have contributed to the minute reduction in spectral response observed from the irradiated spot. Nonetheless, for a broad wavelength range, the absorption remained uniform,

implying that the composite material preserved its ability to generate a reliable response signal.[20,21]

X-ray Photoelectron Spectroscopy. Surface characterization consistently showed Si, B and C elemental peaks from the laser-irradiated areas. The high-resolution peaks were curve-fitted by use of Gaussian-Lorentzian (70:30) mix function and are plotted in Figure 7. The total area under each peak provided an approximation of the respective elemental and phase composition, as summarized in Table 3.

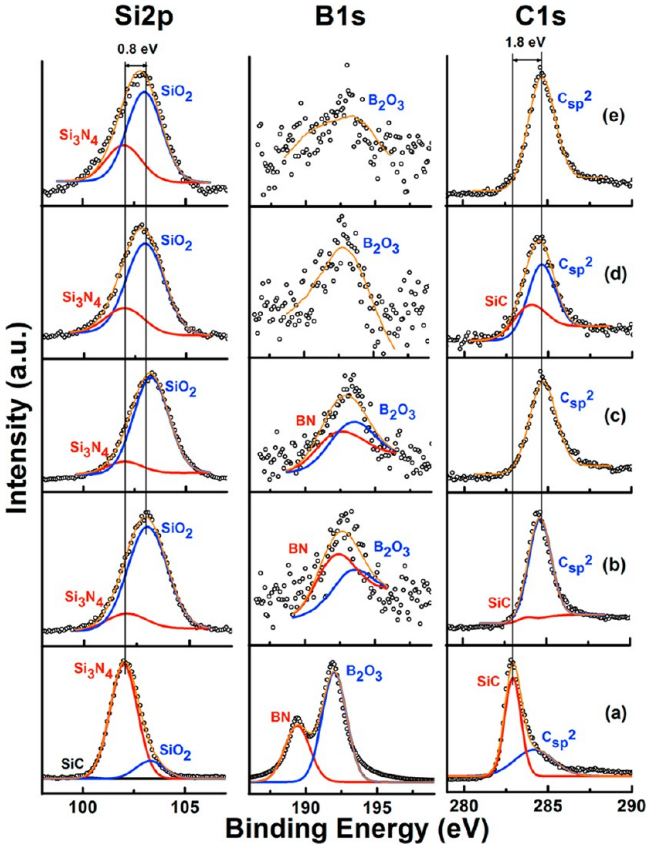

Figure 7. Elemental X-ray photoelectron spectra of Si(B)CN-MWCNT coatings on copper plate specimen exposed to laser irradiance at (a) 0 (unexposed), (b) 4, (c) 8, (d) 12, and (e) 15 kW cm^{-2} for 2 s, respectively.

Table 3. Atomic Composition of Si(B)CN-MWCNT Coating for Unexposed and Irradiated Coating Areas (2 s exposure) for Copper Plate Specimen Obtained Through XPS[a]

	atomic percentage					elemental ratios		
laser power density (kW cm^{-2})	Si	B	C	N	O	Si/B	Si/C	Si/O
unexposed	13.3	6.5	37.8	2.9	39.3	2	0.3	0.3
4	17.8	2.7	40.5		39	6.6	0.4	0.5
8	24.6	2	17.5		55.8	12.3	1.4	0.4
12	25.4	1.8	17.9		54.9	14.1	1.4	0.5
15	20.1	1.6	39		39.3	12.6	0.5	0.5

[a]All atomic percentage measurements are accurate up to approximately 15%.

The deconvolution of Si2p elemental peak from the non-irradiated area showed a sharp peak corresponding to Si−N type bond (due to Si_3N_4 at ∼102 eV) and a smaller peak at a higher energy of ∼103 eV due to Si−O bond. The XPS peaks from laser-irradiated spots exhibited higher electronegativity shift in Si peak from Si−N to Si−O type bonds. The B1s valence elemental peak in the non-irradiated and irradiated spots showed mixed existence of both B−N and B−O type bonds at ∼192.1 and ∼193.1 eV, respectively. The boron peaks in laser-irradiated spots were not clearly recognized, suggesting a decrease in the amount of surface boron. The binding energy of C1s photoelectrons (as a strong and narrow peak) at ∼283.8 eV confirmed the Si−C bond assignment in the non-irradiated specimen. The XPS spectrum from the laser-irradiated areas suggests a diminishing Si−C peak and an emerging sp^2 free-carbon peak (at higher binding energy of ∼284.6 eV).[30] In summary, the XPS analysis confirmed that coating's composition transformed from a Si−C rich phase into a Si−O type phase upon increasing laser irradiance, whereas the graphitic carbon could still be observed in the coating.

CONCLUSION

In conclusion, we have demonstrated preparation of spray coatings composed of core−shell Si(B)CN-MWCNT composite that sustain laser irradiation up to 15 kW cm^{-2} at 10.6 μm for 10 s. Unlike any other thermal absorber coating reported in literature, this composite material shows both the very high optical absorbance and an order-of-magnitude higher damage tolerance. The coatings exposed to incremental laser power density and exposure times were analyzed following various spectroscopic and imaging techniques. Electron microscopy revealed no major destruction i.e., burning, delamination, and deformation for the disk specimen other than some isolated surface discontinuities. Raman spectroscopy suggests the survival of graphitic carbon (and CNTs) in the coating. Direct dependence of irradiation power density on I_D/I_G ratio, suggests systematic evolution of sp^3 carbon from sp^2-bonded-graphitic carbon. XPS results indicate partial oxidation of Si_3N_4/SiC ceramic shell into stable SiO_2 phases and suggest its adaptable nature. Ex situ power reflectance measurements confirmed the high optical absorbance of the coating, 99.87% for the unexposed area and 97.54% for the area that received 15 kW cm^{-2} exposure. The uniform optical absorbance and high damage tolerance of the coating is collectively attributed to the presence of MWCNTs in the core and high oxidation resistance of Si(B)CN ceramic shell, respectively.

ASSOCIATED CONTENT

Supporting Information

Additional SEM images of composite spray coating on the copper plate specimen; results from the ASTM Tape test for measuring coating's adhesion to the copper substrate (along with the media file). This material is available free of charge via the Internet at http://pubs.acs.org.

AUTHOR INFORMATION

Corresponding Author

*E-mail: gurpreet@k-state.edu. Tel.: +1-785-532-7085. Fax: +1-785-532-7057.

Notes

The authors declare no competing financial interest.

ACKNOWLEDGMENTS

This research is based on work supported by the National Science Foundation under Grant EPS-0903806 and the State of

Kansas through Kansas Technology Enterprise Corporation. G.S. thanks Mr. Saksham Pahwa for help with the graphics. Certain commercial equipment, instruments, or materials are identified in this document. Such identification implies neither recommendation nor endorsement by the National Institute of Standards and Technology, or that the products identified are necessarily the best available for the purpose.

REFERENCES

(1) Cromer, C. L.; Hurst, K.E.; Li, X.; Lehman, J.H. *Opt. Lett.* **2009**, *34*, 193−195.
(2) Lehman, J.H.; Dillon, A. *Laser Focus World* **2005**, *41*, 81−87.
(3) Lehman, J. H.; Lee, B.; Grossman, E.N. *Appl. Optics* **2011**, *50*, 4099−4104.
(4) Theocharous, E.; Engtrakul, C.; Dillon, A.C.; Lehman, J. H. *Appl. Opt.* **2008**, *47*, 3999−4003.
(5) Lehman, J.H.; Engtrakul, C.; Gennett, T.; Dillon, A.C. *Appl. Opt.* **2005**, *44*, 483−488.
(6) Lehman, J.H.; Sanders, A.; Hanssen, L.; Wilthan, B.; Zeng, J.; Jensen, C. *Nano Lett.* **2010**, *10*, 3261−3266.
(7) Lehman, J.H.; Hurst, K.E.; Radojevic, A.M.; Dillon, A.C.; Osgood, R.M. *Opt. Lett.* **2007**, *32*, 772−774.
(8) Theocharous, E.; Lehman, J.H. *Infrared Phys. Technol.* **2011**, *54*, 34−38.
(9) Advena, D.J.; Bly, V.T.; Cox, J.T. *Appl. Opt.* **1993**, *32*, 1136−1144.
(10) Blevin, W.R.; Geist, J. *Appl. Opt.* **1974**, *13*, 2212−2217.
(11) Blevin, W.R.; Geist, J. *Appl. Opt.* **1974**, *13*, 1171−1178.
(12) Lehman, J.H.; Theocharous, E.; Eppeldauer, G.; Pannell, C. *Meas. Sci. Technol.* **2003**, *14*, 916−922.
(13) Betts, D.B.; Clarke, F.J.; Cox, L.J.; Larkin, J.A. *J. Phys. E: Sci. Instrum.* **1985**, *18*, 689−696.
(14) Nelms, N.; Dowson, J. *Sens. Actuators, A* **2005**, *120*, 403−407.
(15) Lehman, J.H.; Hurst, K.E.; Roberson, L.K.; Nield, K.; Hamlin, J.D. *J. Phys. Chem. C* **2008**, *112*, 11776−11778.
(16) Chunnilall, C.J.; Lehman, J.H.; Theocharous, E.; Sanders, A. *Carbon*, **2012**, http://dx.doi.org/10.1016/j.bbr.2011.03.031.
(17) Hurst, K.E.; Dillon, A.C.; Yang, S.; Lehman, J.H. *J. Phys. Chem. C* **2008**, *112*, 16296−16300.
(18) Ramadurai, K.; Cromer, C.L.; Li, X.; Mahajan, R.L.; Lehman, J.H. *Appl. Opt.* **2007**, *46*, 8268−8271.
(19) Ramadurai, K.; Cromer, C.L.; Dillon, A.C.; Mahajan, R.L.; Lehman, J.H. *J. Appl. Phys.* **2009**, *105*, 093106.
(20) Ramadurai, K.; Cromer, C.L.; Lewis, L.A.; Hurst, K.E.; Dillon, A.C.; Mahajan, R.L.; Lehman, J.H. *J. Appl. Phys.* **2008**, *103*, 013103.
(21) Theocharous, E.; Deshpande, R.; Dillon, A.C.; Lehman, J.H. *J. Appl. Opt.* **2006**, *45*, 1093−1097.
(22) Bhandavat, R.; Singh, G. *J. Am. Ceram. Soc.* **2012**, *95*, 1536−1543.
(23) Wang, Z.C.; Aldinger, F.; Riedel, R. *J. Am. Ceram. Soc.* **2001**, *84*, 2179−2183.
(24) Riedel, R.; Kienzle, A.; Dressler, W.; Ruwisch, L.; Bill, J.; Aldinger, F. *Nature* **1996**, *382*, 796−798.
(25) An, L.N.; Xu, W.X.; Rajagopalan, S.; Wang, C.M.; Wang, H.; Fan, Y.; Zhang, L.G.; Jiang, D.P.; Kapat, J.; Chow, L.; Guo, B.H.; Liang, J.; Vaidyanathan, R. *Adv. Mater.* **2004**, *16*, 2036−2040.
(26) Shah, S.R.; Raj, R. *J. Eur. Ceram. Soc.* **2005**, *25*, 243−249.
(27) Bill, J.; Aldinger, F. *Adv. Mater.* **1995**, *7*, 775−787.
(28) Papendorf, B.; Nonnenmacher, K.; Ionescu, E.; Kleebe, H.; Riedel, R. *Small* **2011**, *7*, 970−978.
(29) Bhandavat, R.; Kuhn, W.; Mansfield, E.; Singh, G. *ACS Appl. Mater. Interfaces* **2012**, *4*, 11−16.
(30) Tharigen, T.; Lippold, G.; Riede, V.; Lorenz, M.; Koivusaari, K.J.; Lorenz, D.; Mosch, S.; Grau, P.; Hesse, R.; Streubel, P.; Szargan, R. *Thin Solid Films* **1999**, *348*, 103−113.